

FOCUSED ION BEAM MICRO-FABRICATION AND IBIC CHARACTERIZATION OF A MULTI-ELECTRODE DIAMOND DETECTOR WITH BURIED GRAPHITIC ELECTRODES

J. Forneris^{1*}, V. Grilj², M. Jakšić², N. Skukan², C. Verona³, G. Verona-Rinati³, A. Lo Giudice¹, P. Olivero¹, F. Picollo¹, E. Vittone¹

¹ Physics Department, and NIS Excellence Centre - University of Torino; INFN - sez. Torino; CNISM - sez. Torino; via P. Giuria 1, 10125 Torino, Italy

² Ruđer Bošković Institute, Bijenicka 54, P.O. Box 180, 10002 Zagreb, Croatia

³ Dipartimento di Ingegneria Industriale, Università di Roma “Tor Vergata”, Via del Politecnico 1, 00133 Roma, Italy

*forneris@to.infn.it

Introduction

The Deep Ion Beam Lithography (DIBL) microfabrication of monocrystalline diamond [1] consists of a selective damage introduction in the crystal by means of MeV ion beams focused down to a micrometer spot size and raster scanned on the sample along predefined patterns.

The damage induced by ions is localized mainly at their end of range, i.e. a few micrometers below the surface. The regions, in which the vacancy density overcomes a critical “graphitization threshold”, convert to a graphitic phase upon thermal treatment. Elsewhere, the diamond structure is recovered to a large extent.

This method allows to define highly conductive graphitic channels in single crystal diamond, whose length is limited by the range of the ion microbeam scanning system (several hundred micrometers), whose width is given by the beam spot size, and whose formation depth is defined by the nuclear stopping range of the ions (few micrometers).

The production of highly conductive, optically opaque, chemically reactive graphitic structures embedded in a highly resistive, optically transparent and chemically inert diamond matrix is of potential interest for many applications, e.g. for the realization of diamond 3D microstructures [2], microfluidic channels, innovative biosensors [3], IR emitters [4], bolometers [5]. Moreover, the DIBL technique can be exploited to realize novel 3D architectures for ionizing radiation detection with enhanced radiation hardness properties.

The Ion Beam Induced Charge (IBIC) [1] microscopy was identified as the most suitable technique in order to characterize and map at the micrometric level the electronic properties and the charge collection efficiency (CCE) of micro-fabricated diamond detectors.

CCE maps obtained by raster scanning a 4 MeV He ion micro-beam onto the sample surface provided information not easily available otherwise on the electronic characteristics of the detector, such as the electric field geometry, the role of carrier species in the induced charge pulse formation and the evaluation of the residual damage introduced by the DIBL fabrication in the diamond lattice.

Experimental

The sample under test (sample 1) consisted of an intrinsic homoepitaxial single-crystal $\sim 40 \mu\text{m}$ thick diamond layer grown on a HPHT Ib single crystal substrate at the Rome “Tor Vergata” University, by means of a Microwave Plasma

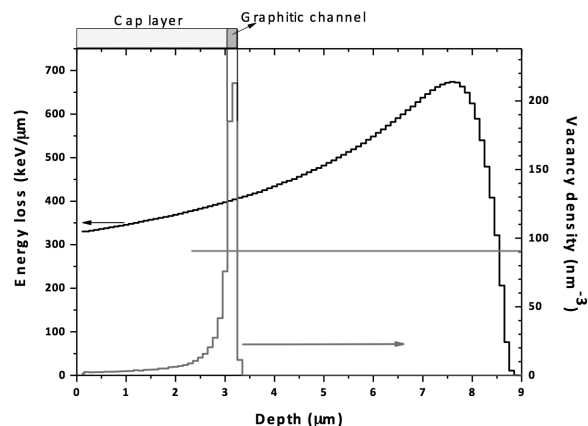


Figure 1. Energy loss of 4 MeV He⁺ ions in diamond (left scale) and vacancy density profile in diamond generated by $1.47 \cdot 10^{17}$ He⁺ ions of energy 1.8 MeV (right scale) as evaluated by SRIM 2011 simulation. The horizontal line indicates the graphitization threshold [7].

Enhanced Chemical Vapour Deposition process [8].

Graphitic channels were made by DIBL [1] at the INFN National Laboratories of Legnaro (I), using a 1.8 MeV He ion microbeam. The ion fluence was $\sim 1.5 \cdot 10^{17} \text{ cm}^{-2}$, which is sufficient, according to SRIM2011 simulations [9], to produce a vacancy density profile with a damage peak above the graphitization threshold [12] at a depth of $\sim 3 \mu\text{m}$ (Fig. 1).

The evaporation of slowly-thinning Cu masks onto the diamond surface before implantation allowed for the modulation of the depth of the damaged channels, ensuring their electrical continuity with the surface.

After ion implantation, the sample was annealed in vacuum at 1100 °C for 2 hours, in order to both convert the highly-damaged regions to a graphitic phase and to recover the sub-threshold structural damage introduced in the “cap layer” overlying the above-mentioned damaged region (i.e., the region overlying the buried channels [1]).

The DIBL process resulted in the fabrication of four parallel buried graphitic channels (see Fig. 2a), plus an additional orthogonal channel, Each channel was $\sim 10 \mu\text{m}$ wide, the average spacing being $\sim 12 \mu\text{m}$. Due to the homoepitaxial growth process, the sample was not equipped with a back electrode.

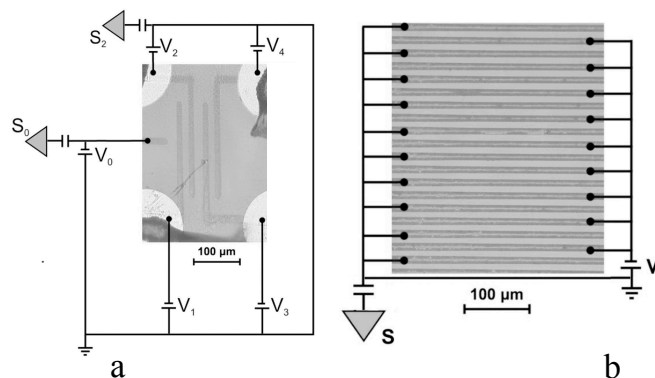


Figure 2. Optical micrograph of: (a) Sample 1, the graphitic channels buried in the diamond matrix are visible as opaque stripes; (b) Sample 2, equipped with surface interdigitated Ti/Pt/Al electrodes. Relevant connections to the amplification/bias circuits are sketched.

The emerging endpoints of the channels at the surface were contacted to perform electrical measurements. The current measured between any pair of electrodes was below the detection limit of our electrometer (<1 pA at ± 100 V applied bias), showing both the high resistivity of the diamond matrix surrounding the channels and a negligible surface leakage current.

An additional, nominally identical diamond sample (sample 2) was grown to provide a comparison between buried graphitic channels and standard ohmic surface metallic contacts (Fig. 2b). The sample was equipped with Ti/Pt/Au (50/20/50 nm) finger contacts patterned by means of a standard lift-off photo-lithographic technique [10]. The current flowing between the two fingers was below the instrumental sensitivity (i.e. < 1 pA at ± 100 V).

IBIC measurements were performed at the Ruđer Bošković Institute (RBI) using a $4 \mu\text{m}$ spot size 4 MeV He in order to probe the region below the graphitic electrodes (penetration depth: $\sim 9 \mu\text{m}$, Fig. 1).

Sample 1 was investigated through a low current (< 1000 ions $\cdot\text{s}^{-1}$, to prevent damage and pile-up effects) microbeam raster scan of a rectangular area ($120 \times 150 \mu\text{m}^2$) surrounding the buried electrodes. Pulse height processing, beam scanning and 2D map acquisition was carried out by a hardware and software system developed at the RBI [11].

Sample 2 was analysed using the same IBIC set up; the ion beam scan area was set to about $300 \times 300 \mu\text{m}^2$.

Results

Fig. 3a shows the IBIC map collected from sample 1 by the the sensitive electrode S_0 (Fig. 2a) polarized at $+80$ V, when the other vertical electrodes are grounded. Charge pulses above the electronic threshold (7.5% CCE) are generated only close to the sensitive electrode; the motion of free carriers generated elsewhere does not induce any detectable signal, as evidenced by the the CCE profile along the horizontal direction centered in the middle of the horizontal electrode.

When the applied bias is inverted to -80 V (Fig. 3b), the IBIC map shows a complementary result, in which no pulses are detected close to S_0 electrode. Detectable pulses are generated in the area surrounding the four vertical grounded electrodes, as highlighted by the CCE horizontal profile.

The IBIC theory provides a satisfactory interpretation of these results [6]. Assuming a perfect intrinsic material with ideal ohmic contacts, the traditional approach based on Ramo's theorem relying on the evaluation of the weighting potential can be adopted. The weighting potential is mapped by solving the Laplace's equation assuming a unit potential at the sensitive electrode while all the other electrodes are grounded. This approach allowed us to identify the region where detectable charge pulses are generated, whose intensity is proportional to the difference in weighting potential between the initial and final position of the moving charge carriers [1].

The weighting potential maps relevant to the sensitive electrode S_0 by means of a Finite Element Method solver [1] are shown in Fig. 4a, 4b; the streamlines indicate the trajectories of positive charges according to the electrostatic field generated by the bias configurations relevant to Figs. 3a and 3b, respectively.

The role of electrons and holes in the pulse formation can be understood by comparing the weighting potential with the experimental IBIC maps. In Fig. 3a the pulses arise in proximity of the anode.

Electrons provide a negligible contribution to the CCE since

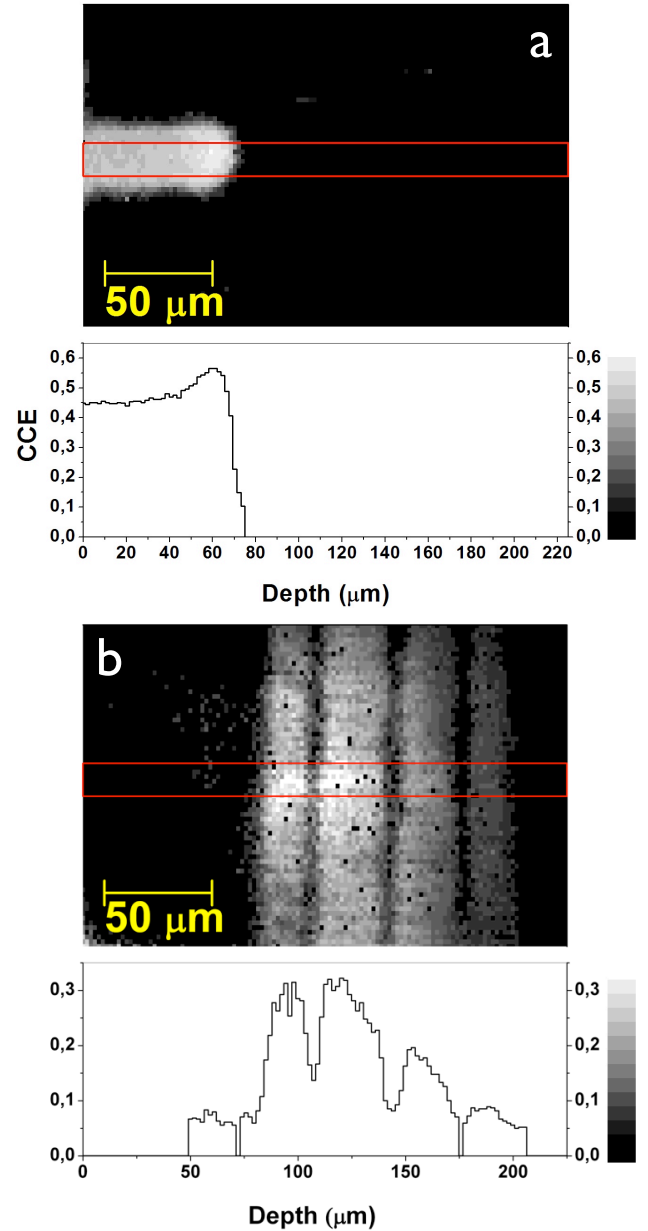


Figure 3. IBIC map from sample 1 collected under the following bias conditions: (a) $V_0=+80$ V; $V_1=V_2=V_3=V_4=0$ V. (b) $V_0=-80$ V; $V_1=V_2=V_3=V_4=0$. In both cases, the sensitive electrode is S_0 (ref. Fig. 2). Below, horizontal CCE median profiles along the rectangular regions highlighted in red.

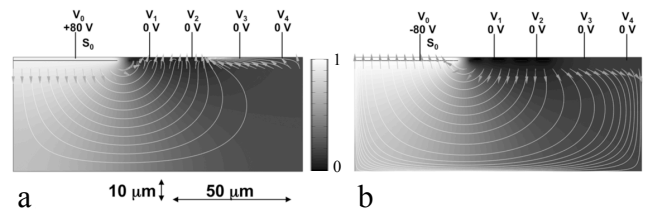


Figure 4. Weighting potential maps and electric field streamlines relevant to the IBIC maps shown in Fig. 3a (a) and 3b (b). The streamlines are generated at a depth of $8 \mu\text{m}$, corresponding to the maximum of the ionization curve. Arrows indicate the electric field at the generation points.

they are collected by S_0 crossing a region with a nearly constant weighting potential; holes drift towards the grounded electrodes spanning regions with weighting potential ranging from almost 1 to 0 (Fig. 4a).

If charge generation occurs near a grounded electrode(s), electrons should provide a dominant contribution; however the CCE profile (Fig. 3a) is zero, indicating that their drift length (and hence their lifetime) is significantly shorter than the distance between the electrodes.

Such an interpretation is confirmed by the results in Fig. 3b, where the bias polarity is inverted and holes generated at the anodes (vertical electrodes) move towards the sensitive electrodes, having a drift length sufficient to cross regions with a pronounced variation in weighting potential (Fig. 4b). Fig. 5a shows the CCE map and the relevant horizontal profile collected by the second vertical electrode (S_2) under the following biasing conditions: V_0, V_2, V_4 grounded and V_1, V_3 at -100 V. As expected, only the region around the S_2 electrode (anode) provides a detectable signal; the profile has a maximum of $\sim 60\%$ CCE and a FWHM of about 30 μm .

Such a configuration was adopted to provide a comparison with IBIC maps (Fig. 5b) acquired in similar bias conditions on sample 2 (Fig. 2b), equipped with metallic electrodes deposited in a comb-like structure onto the diamond surface. The CCE profile shows that at the centre of each tooth-comb, the efficiency reaches a value of 80% , remarkably higher than that in Fig. 5a. According to Fig. 1, about 25% of the carriers are generated in the cap layer. Such a difference can be then ascribed to sub-threshold damage induced by DIBL, sufficient to prevent a full recovery of the electronic

properties of the diamond sample and resulting in the hole trapping in the cap layer [12].

Conclusions

The IBIC characterization of a CVD diamond detector with buried graphitic electrodes fabricated by DIBL was performed.

From the point of view of the material qualification, IBIC maps evidenced that detectable charge signals were formed mainly at the anodes, independently of the different electrical configurations adopted in the measurements. The experimental results are compatible with a model which considers holes as the dominant carrier specie contributing to the induced charge formation mechanism, as already observed by other authors by induced transient current measurements [13]. The low contribution of electrons transport can be ascribed to carriers trapping, resulting in short average lifetime.

From the point of view of the fabrication process qualification, IBIC measurements highlighted a residual damage induced during DIBL processing, which was only partially healed by thermal annealing. Residual trapping centres strongly reduced the carrier (hole) lifetimes (few ps), making the cap layer almost inactive for the detection of ionizing radiation.

From the point of view of the detector's performance qualification, the electrical configuration adopted in Fig. 4b provided a wide active area ($\sim 200 \times 200$ μm^2) for ionizing radiation detection. Furthermore, as shown in Fig. 5a, the multi-electrode structure of the device allows one to use each buried channel as a sensitive electrode. Such a feature could be exploited in future activities in order to provide position sensitivity for the ionizing radiation detection at the micrometric level in an innovative full-carbon detector.

Acknowledgements

This work was supported by INFN experiment DIAMED; by European Community as an Integrating Activity 'Support of Public and Industrial Research Using Ion Beam Technology (SPIRIT)' under EC contract no. 227012; by MIUR, PRIN2008 National Project "Synthetic single crystal diamond dosimeters for application in clinical radiotherapy"; and by University of Torino "Progetti di Ricerca di Ateneo-Compagnia di San Paolo-2011- Linea 1A, progetto ORTO11RR5".

References

- [1] Olivero P, Forneris J, Jakšić M, Pastuovic Z, Picollo F, Skukan N, Vittone E, Nucl. Instr. Meth. B 269 (2011) 2340.
- [2] Olivero P, Rubanov S, Reichart P, Gibson CC, Huntington ST, Rabeau J, Greentree AD, Salzman J, Moore, Jamieson DN, Praver S, Advanced Materials 17 (2005) 2427.
- [3] Picollo F, Gatto Monticone D, Olivero P, Fairchild BA, Rubanov S, Praver S, Vittone E, New Journ. Phys. 14, (2012) 053011.
- [4] Praver S, Devir AD, Balfour LS, Kalish R, Appl. Opt. 34 (1995) 636.
- [5] Galkina TI, Klokov AY, A. Sharkov I, Khmel'nitskii RA, Gippius AA, Dravin VA, Ral'chenko VG, Savel'ev AV, Physics of the Solid State 49 (2007) 654.
- [6] Breese MBH, Vittone E, Vizkelethy G, Sellin PJ, Nucl. Instr. Meth. B 264 (2007) 345.
- [7] Kalish R, Praver S, Nucl. Instr. Meth. Phys. Res. B 106 (1995) 492.
- [8] Almaviva S, Marinelli M, Milani E, Prestopino G,

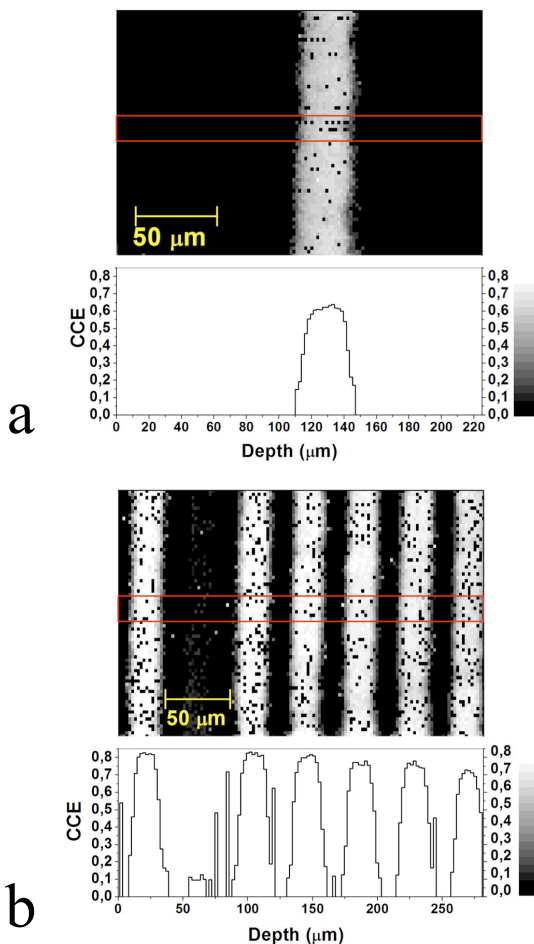


Figure 5. IBIC map and relevant horizontal profile of (a) sample 1 under the following bias condition: $V_0=V_2=V_4=0$; $V_1=V_3=-100$ V. The sensitive detector is S_2 (Fig. 2a). (b) sample 2; the sensitive comb is grounded and the other is at -100 V (Fig. 2b).

- Tucciarone A, Verona C, Verona-Rinati G, Angelone M, Pillon M, Nucl. Instr. Meth. A 612 (2010) 580.
- [9] Ziegler JF, Ziegler MD, Biersack JP, Nucl. Instr. Meth. B, 268 (2010) 1818.
- [10] Werner M, Semicond. Sci. Technol, 18 (2003) S41-6.
- [11] Bogovac M, Jakšić M, Wegrzynek D, Markowicz A, Nucl. Instr. Meth. B 267 (2009) 2073.
- [12] Baskin E, Reznik A, Saada D, Adler J, Kalish R, Phys. Rev. B 64 (2001) 224110.
- [13] Pomorski M, Berdermann E, Caragheorghopol A, Ciobanu M, Kiš M, Martemiyarov A, Nebel C, Moritz P, Phys. Stat. Sol. A 203 (2006) 3152.